ARTICLE
Journal of Cellular Biochemistry 114:2258–2272 (2013)

Journal of Cellular Biochemistry

The Leading Role of Microtubules in Endothelial Barrier Dysfunction: Disassembly of Peripheral Microtubules Leaves Behind the Cytoskeletal Reorganization

Irina B. Alieva,[1,2,3]* Evgeny A. Zemskov,[3] Ksenija M. Smurova,[1] Irina N. Kaverina,[4] and Alexander D. Verin[3]

[1]*Electron Microscopy Department, A.N. Belozersky Institute of Physico-Chemical Biology, Moscow State University, Moscow, Russia*

[2]*Department of Histology, Cytology and Embryology, Medical Faculty People's Friendship University of Russia, Mikluho-Maklaya str. 6, Moscow, Russia*

[3]*Vascular Biology Center, Georgia Health Sciences University, Augusta, Georgia, 30912*

[4]*Department of Cell and Developmental Biology, Vanderbilt University Medical Center, Nashville, Tennessee, 37232*

ABSTRACT

Disturbance of the endothelial barrier is characterized by dramatic cytoskeleton reorganization, activation of actomyosin contraction and, finally, leads to intercellular gap formation. Here we demonstrate that the edemagenic agent, thrombin, causes a rapid increase in the human pulmonary artery endothelial cell (EC) barrier permeability accompanied by fast decreasing in the peripheral microtubules quantity and reorganization of the microtubule system in the internal cytoplasm of the EC within 5 min of the treatment. The actin stress-fibers formation occurs gradually and the maximal effect is observed relatively later, 30 min of the thrombin treatment. Thus, microtubules reaction develops faster than the reorganization of the actin filaments system responsible for the subsequent changes of the cell shape during barrier dysfunction development. Direct microtubules depolymerization by nocodazole initiates the cascade of barrier dysfunction reactions. Nocodazole-induced barrier disruption is connected directly with the degree of peripheral microtubules depolymerization. Short-term loss of endothelial barrier function occurs at the minimal destruction of peripheral microtubules, when actin filament system is still intact. Specifically, we demonstrate that the EC microtubule dynamics examined by time-lapse imaging of EB3-GFP comets movement has changed under these conditions: microtubule plus ends growth rate significantly decreased near the cell periphery. The microtubules, apparently, are the first target in the circuit of reactions leading to the pulmonary EC barrier compromise. Our results show that dynamic microtubules play an essential role in the barrier function in vitro; peripheral microtubules depolymerization is necessary and sufficient condition for initiation of endothelial barrier dysfunction. J. Cell. Biochem. 114: 2258–2272, 2013.

KEY WORDS: HUMAN PULMONARY ENDOTHELIUM; ENDOTHELIAL BARRIER FUNCTION; ENDOTHELIAL BARRIER DYSFUNCTION; MICROTUBULES; MICROTUBULE DYNAMICS

Lining the inner surface of blood vessels, the endothelium fulfils a specific barrier function. It controls the permeability of the vascular wall and exchange of metabolites and nutrients between circulating blood and tissue liquid. This function is regulated by the cytoskeleton contractile and stretching forces existing at equilibrium in intact endothelium [Lum and Malik, 1996; Dudek and Garcia, 2001; Bogatcheva et al., 2002; Birukova et al., 2004a,b; Mehta and Malik, 2006; Shivanna and Srinivas, 2009]. The cytoskeleton reorganization can change the cell shape to provoke intercellular gap formation and provides structural basis for a hyperpermeability, the main cause of vascular endothelial dysfunction. This phenomenon is common for a number of pathological states and diseases

Grant sponsor: Russian Foundation for Basic Research; Grant numbers: 09-04-00363, 12-04-00488; Grant sponsor: GHSU CVDI and American Heart Association; Grant number: 11SDG7670035; Grant sponsor: NIH; Grant numbers: HL067307, HL080675, HL101902, R01-GM78373; Grant sponsor: American Heart Association Grant-in-Aid; Grant number: 10GRNT4230026.

*Correspondence to: Irina B. Alieva, Electron Microscopy Department, A.N. Belozersky Institute of Physico-Chemical Biology, Moscow State University, Moscow, Russia. E-mail: irina_alieva@belozersky.msu.ru

Manuscript Received: 19 December 2012; Manuscript Accepted: 11 April 2013

Accepted manuscript online in Wiley Online Library (wileyonlinelibrary.com): 19 April 2013

DOI 10.1002/jcb.24575 • © 2013 Wiley Periodicals, Inc.

(inflammation, asthma, sepsis, acute lung injury, ischemia, diabetes) and can lead to severe, and even fatal, organ dysfunction [Garcia et al., 1995; Lum and Malik, 1996; van Nieuw Amerongen et al., 2000; Dudek and Garcia, 2001; Groeneveld, 2002; Komarova et al., 2007; Jalimarada et al., 2009], as well as a complication upon the treatment, for example, by a number of anti-cancer pharmacologic drugs [Cattan and Oberg, 1999; Jordan and Wilson, 2004; Pasquier et al., 2005; Schwartz, 2009]. The knowledge of the barrier dysfunction mechanisms and their triggering elements is critical to prevent the drug side-effects. It is logical to assume a possibility to avoid the development of the endothelial dysfunction by protection the very first structural element affected in the cascade leading to the intercellular gap formation. In our opinion, a search for such pharmacological protectors is crucial for cure of vascular diseases.

Microtubules and the actin cytoskeleton function in cooperation in normal endothelium and under conditions of the barrier loss. Their coordination is accomplished at several levels by cross-linker proteins which join microtubules and actin filaments [Fuchs and Karakesisoglou, 2001; Rodriguez et al., 2003; Bershadsky et al., 2006], as well as by small GTPases of the Rho family which mediate dynamics and organization in both the actin network and microtubules [Cook et al., 1998; Daub et al., 2001; Fukata et al., 2002; Ishizaki et al., 2001; Jaffe and Hall, 2005; Palazzo et al., 2001]. Earlier we described a cellular model established in physiologically-relevant human pulmonary artery EC (HPAEC) [Alieva et al., 2010]. This cellular model expressing EB3-GFP is indispensable to study the involvement of microtubules in the barrier-protective/compromising mechanisms activated in pulmonary endothelium by pharmacological agents of interest as well as by specific cytoskeleton inhibitors. Our previous data demonstrated the critical involvement of the microtubule disassembly in induced EC barrier dysfunction [Birukova et al., 2004a,b; Smurova et al., 2008] and suggested that microtubule dynamics is an early event in the circuit of the reactions leading to the changes in pulmonary EC barrier permeability [Smurova et al., 2008]. The present work reveals a consistency of cytoskeletal components reactions in the endothelial barrier dysfunction and defines a role of dynamic microtubules in this process.

MATERIALS AND METHODS

CELL CULTURE AND TREATMENTS

Human pulmonary artery EC (HPAEC) were obtained from Clonetics BioWhittaker Inc. (Clonetics BioWhittaker, San Diego, CA) and were grown in complete EGM-2 medium (Clonetics BioWhittaker) at 37°C in an atmosphere of 5% CO_2. Experiments were performed on the cell cultures at 6–10th passages, seeded at ≈30% confluence, and utilized at ≈80–100% confluence depending on the type of experiments.

Thrombin (Sigma, St. Louis, MO) concentrations: 25 and 50 nM for electrical cell substrate impedance sensing system (ECIS) studies and 25 nM for all other experiments. Before the treatment, the cells were washed with serum-free medium. The cells were incubated with thrombin in serum-free medium for 5, 10, 30, and 60 min. Nocodazole (Sigma) concentrations: 50, 100, 200, and 500 nM for ECIS and 100 or 200 nM for all other experiments. Rho-kinase inhibitor Y-27632 (Tocris, Ellisville, MO) concentration: 5 μM. The cells were incubated with Y-27632 for 1 h. Nocodazole and Y-27632 stock solutions were prepared in DMSO. Final concentrations of DMSO in the cell medium did not exceed 0.1%.

MEASUREMENT OF TRANSENDOTHELIAL ELECTRICAL RESISTANCE

To characterize the endothelial barrier capacity, a highly sensitive method of registration of the EC monolayer electrical resistance using ECIS equipment (electrical cell substrate impedance sensing system) (Applied Biophysics, Troy, NY) was used. HPAEC were seeded in special ECIS arrays. Measurements of transendothelial electrical resistance (TER, an index of EC monolayer integrity) through confluent monolayer were performed as described previously [Verin et al., 2001; Birukova et al., 2004b].

EXPRESSION PLASMIDS AND TRANSFECTION

Plasmids encoding constitutively active mutants Gα12-Q229L and Gα13-Q226L were kindly provided by Prof. T. Voyno-Yasenetskaya (University of Illinois at Chicago, Chicago, IL) and used for transient transfections [Voyno-Yasenetskaya et al., 1994]. HPAEC grown in 12-well plates at 60% confluence were transfected with plasmid DNA (1 μg) using Fugene 6 (Boehringer Mannheim-Roche, Indianapolis, IN) as described earlier [Birukova et al., 2004a]. After 30 h of the transfection, the cells were used in the experiments. Control cells were transfected with empty vectors.

To calculate the microtubule growth rate in living HPAEC, the cells were transfected with expression vector encoding EB3-GFP (kind gift of Prof. A. Akhmanova [Akhmanova et al., 2001]), which serves as a marker of growing distal tips (plus-ends) of microtubules [Stepanova et al., 2003]. Effectene transfection reagents (Qiagen Inc., Hilden, Germany) were used for the transfection of the EB3-GFP plasmid into HPAEC according to the manufacturer's protocol. Transfected cells were selected for image analysis by detecting GFP fluorescence.

IMMUNOFLUORESCENCE AND LIVE CELL IMAGING

Prior to immunofluorescence staining, HPAEC grown on glass coverslips were fixed for 10 min with methanol (−20°C) or 15 min with a 1.5% solution of glutaraldehyde (Sigma) in phosphate-buffered saline (PBS), pH 6.8 (Sigma) at room temperature (RT) and washed three times with PBS (10 min for each washing). Fixed cells were permeabilized with 0.1% Triton X-100 (Sigma) in PBS for 15 min and washed three times with PBS for 10 min. To avoid background fluorescence, the cells were treated with a 1% solution of sodium borohydride ($NaBH_4$) (Sigma) in PBS (10 min, three times) and washed three times with PBS for 10 min prior to the incubation with antibodies. Treated cells were incubated with mouse monoclonal antibodies to β-tubulin (Covance, Princeton, NJ), (dilution 1:200), and then with secondary antibodies. Incubation with antibody of interest was performed in blocking solution (2% BSA in PBS) for 30 min, 37°C, followed by incubation with Alexa 488-conjugated secondary antibodies (Molecular Probes, Eugene, OR) (dilution 1:100, 30 min, 37°C). Actin filaments were visualized using Texas Red-conjugated phalloidin (Molecular Probes) for 1 h at RT. Then, the glass slides were mounted using mounting medium (Kirkegaard and Perry Laboratories, Gaithersburg, MD) and analyzed using Nikon video-imaging system consisting of an inverted microscope Nikon Eclipse TE300 with epi-fluorescence module (Nikon Instech Co., Japan) using

60×A/1.40 oil objective connected to SPOT RT monochrome digital cooled camera Hamamatsu ORCA-2 (Hamamatsu Photonics, Japan) with MetaView software (Universal Imaging, Burbank, CA) and image processor (Diagnostic Instruments, Sterling Heights, MI). The images were acquired using SPOT 3.5 acquisition software (Diagnostic Instruments) and processed with Adobe Photoshop 7.0 (Adobe Systems, San Jose, CA) and Adobe Illustrator CS (Adobe Systems) software. Resolution of recorded images (12 bits) was 9 pixels/μm.

For quantitative analysis of microtubules we proportionally increased a contrast on images of peripheral microtubules in control and treated EC thus minimizing potential errors in the identification of the individual microtubules on the cell periphery. It allows clear identification of microtubule ends on the cell periphery, where lamella is thin and single microtubule image may have a low contrast. Further, this approach allows convincingly demonstrating the absence of peripheral microtubules and facilitating detection of existing individual microtubules on the cell periphery.

VIDEO MICROSCOPY OF EB3-GFP-TRANSFECTED CELLS

Live cells plated on MatTech glass bottom dishes were maintained at 37°C by heated stage (Warner Instruments) on a Nikon TE2000E inverted microscope equipped with a PerfectFocus automated focusing system. Single-plane time-lapse video sequences were taken every 5 s using PLAN APO 100× TIRF oil lens NA 1.49 and a backilluminated EM-CCD camera Cascade 512B (Photometrics, Tucson, AZ) driven by IPLab software (Scanalytics, Rockville, MD). A Pinkel triple-filter set (Semrock, Rochester, NY) was used for nearly simultaneous two-color wide-field imaging.

IMAGE AND VIDEO ANALYSIS

The values were statistically processed using Sigma Plot 7.1 (SPSS Science) software. Quantitative analysis of microtubules was carried out as described previously and included a measurement of the fluorescence using the MetaMorph software (Universal Imaging) and analysis of digital images collected with a digital CCD camera [Birukova et al., 2004a,b]. For the analysis, extended focus images of well-spread cells with minimal thickness were selected. Microtubule subpopulations in the area of interest were computed by the original image segmentation with threshold set to 200% of background level and by calculating the percentage of above-the-threshold pixels. The relative area occupied by the microtubule network in different cell compartments was calculated in three different areas: (1) an area circumjacent to the cell periphery (5 μm from the cell margin); (2) an area circumjacent to the cell periphery (10 μm from the cell margin); and (3) the inner compartment, that is, the internal cytoplasm (10 μm from the cell margin) not including the first two areas. The ratio between the area occupied by microtubules to the measured area was determined separately for each measured area. Similar technique was used to monitor stress fiber formation. Actin fibers were marked out and the ratio of the cell area covered by stress fibers to the whole cell area was determined. The gap formation was expressed as a ratio of the gap area to the area of the whole image. Statistical analysis was performed using Sigma Plot 7.1 (SPSS Science) and Excel (Microsoft Corp., Redmond, WA). Sigma Plot 7.1 software was used for graphical data presentation.

Microtubule system organization in the HPAEC internal cytoplasm was evaluated using MetaMorph (Universal Imaging) software according to the method reported previously [Smurova et al., 2007; Smurova et al., 2004]. The method is based on the measurements of microtubule fluorescence intensity in cell preparations obtained in 10 square areas: from the centrosome (measurement region 1) to cell edge (measurement region 10).

For the quantitative evaluation of individual microtubules on the cell periphery, HPAEC with well-defined thin lamella were selected. All microtubules crossing a random line distant from the edge inside the cell for 5, 10, and 20 μm were counted. Areas with clearly visualized microtubules were used for counting. The value equal to the number of microtubules crossing the random line per 1 μm of its length was estimated as the criterion for the analysis. It is an objective test of microtubule network density, that is, of their occurrence. Rarely, twisted microtubules crossed the random line twice or more. These microtubules were taken into account only once. The data were plotted as criterion-thrombin treatment time diagrams.

Quantitative analysis of the microtubule dynamics was carried out on time-lapse movies of HPAEC expressing EB3-GFP, to label microtubules plus ends [Alieva et al., 2010]. Microtubule growth rates were obtained by tracking EB3-GFP comets at microtubule plus-ends (1 s/frame) using ImageJ software, linked to an Excel spreadsheet. Statistical analysis was performed using Sigma Plot 7.1.

STATISTICS AND DATA PLOTTING

Data obtained were analyzed statistically using ImageJ, Sigma Plot 7.1 and Excel software. Sigma Plot 7.1 was used for data plotting. Diagram approximation was done with Sigma Plot 7.1 and Table Curve 2D 5.1 (Systat Software, Inc.) software.

RESULTS

THROMBIN REGULATES PERMEABILITY OF EC MONOLAYERS IN VITRO

The transendothelial electric resistance (TER, an index of EC monolayer integrity) dramatically declined and gradually restored in thrombin-treated EC, and the rate and the extent of the recovery was dose-dependent [Birukova et al., 2004a,b]. Recovery of TER after 100–200 nM thrombin treatment occurred very slowly and never restored completely [Birukova et al., 2004c]. At 25–50 nM thrombin, the TER dropped more than twice during 10–15 min of the treatment; the increase that appeared in the monolayer permeability defined the EC barrier dysfunction (Fig. 1A). TER was recovered up to 70–80% within 2.5–3 h. This effect of thrombin was dose-dependent, and the recovery of the endothelial barrier to the physiological extent was faster at 25 nM thrombin. Upon 50 nM thrombin treatment, the TER declined and slowly restored; EC monolayer lost cell–cell contacts completely (TER decreased from 1 to 0.2) (Fig. 1A). At these conditions, in the absence of cell–cell contacts, microtubule dynamics was not normal, but similar to that in single cells [Alieva et al., 2010]. Lower concentrations of thrombin did not destroy EC monolayer (TER decreased from 1 to 0.5) (Fig. 1A), and microtubule dynamics was similar to that in the EC maintained neighbor cell contacts. Therefore, in contrast to our previous studies [Birukova et al., 2004c], 25 nM thrombin was selected for current work to induce a rapid but

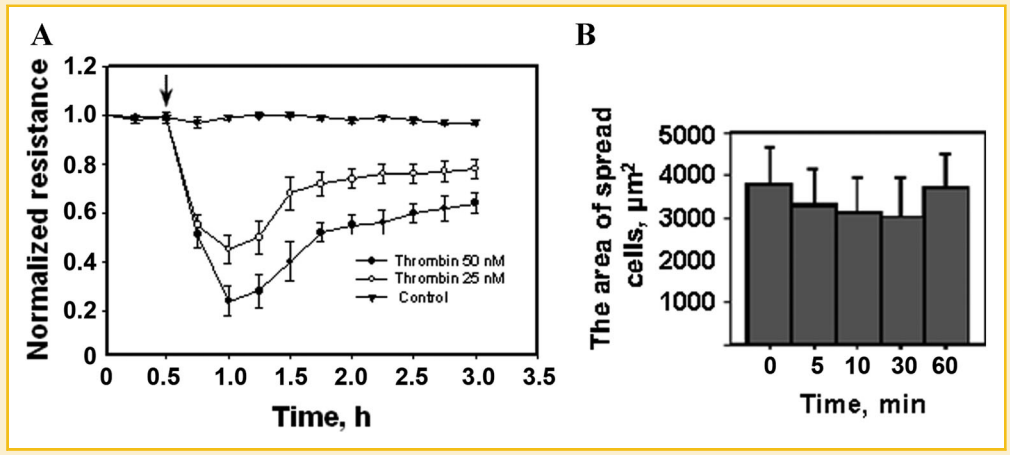

Fig. 1. Effect of thrombin treatment on HPAEC barrier function. A: HPAEC were plated on gold microelectrodes and were cultured to confluence. Growth medium was replaced with serum-free medium, and after equilibration and stabilization, TER was monitored for 3 h. At the time-point indicated by the arrow, HPAEC were treated with thrombin (25 or 50 nM). B: Effect of thrombin on the spread cell area. HPAEC were treated with thrombin (25 nM) for 5, 10, 30, and 60 min; control cells (0 min) were not treated with thrombin. Quantitative analysis was performed using MetaMorph software as described in Materials and Methods Section. Data presented as mean ± SD (n = 3).

reversible endothelial barrier dysfunction (i.e., to analyze the EC barrier capable of rapid recovery after the treatment).

Importantly, the area with the spread cells decreased upon thrombin treatment (Fig. 1B) and the EC cytoskeleton was disturbed (these disturbances will be described in detail further in the text) (Fig. 2A,B). However, the injury of the monolayer was reversible: 60 min after the treatment, the area with spread cells was close to the initial state (Fig. 1B), suggesting that the effector concentrations used in our experiments were comparable to physiological ones.

Similar to the vascular endothelium in vivo, the EC monolayers in our in vitro model were able to adapt to the action of natural regulator, thrombin, at these concentrations (25–50 nM) despite the dramatical cytoskeletal reorganization. This allowed us to monitor a pivotal role of distinct cytoskeleton components in reversible endothelial dysfunction.

MICROTUBULE SYSTEM REORGANIZATION ADVANCES THE ACTIN SYSTEM REACTION IN THROMBIN-INDUCED BARRIER DYSFUNCTION

In normal HPAEC, the microtubule system has a strongly pronounced convergence in the centrosome region. Close to the cell edge, microtubule density decreased significantly, allowing to identify and quantitatively analyze distal microtubule ends, long microtubule fragments, and even individual microtubules in lamella. The thrombin stimulation disturbed the actin and the microtubules organization (Fig. 2A). The treatment led to gradual increase in total stress fiber formation, with a maximum at 30 min of the treatment (Fig. 2A,B), then their quantity decreased, and returned to the control level after 60 min.

The relative area occupied by microtubules was decreased by 25% after 5 min of the treatment (Fig. 2B). Then, the microtubules area was enlarged and was close to the control level at 60 min of the treatment, suggesting a gradual adaptation.

The number of microtubules on the lamella edge of control EC and the cells treated with thrombin for various time periods presented in Figure 2C–F. As the evaluation criterion, we used the number of microtubules that crossed a line of standard length (1 μm) extending from the edge to the inside of the cell at distances of 5, 10, and 20 μm. Data presented in Figure 2C show that the number of peripheral microtubules in control cells depended on the distance to the external cell membrane: the number of microtubules at a distance of 5 μm from the edge was 1.5 and 2.5 times less than those at distances of 10 and 20 μm, respectively. The number of microtubules in these areas varied depending on the duration of the thrombin treatment. In close proximity to the cell edge (5 μm from the external membrane), the relative number of microtubules diminished fourfold after 5 min of the thrombin treatment (Fig. 2C). The decline in this area was the most prominent. Increased time of the treatment resulted in a gradual augmentation of the microtubules. After 60 min of the treatment, the number of microtubules reached the control value (Fig. 2F). Within a 10 μm distance of the external membrane, the number of microtubules decreased three times in the first 5 min of the treatment (Fig. 2C). Later, the gradual recovery of microtubule density was observed. Moving 20 μm away from the cell edge, the number of microtubules diminished twofold in the first 5 min of the thrombin treatment and continued to decrease for the next 5 min (Fig. 2C,D) followed by a recovery up to 80% of the control number of microtubules after 60 min (Fig. 2F). Thus, the decrease in numbers of microtubules was the most obvious within 5 μm of the external cell membrane after 5 min of the thrombin treatment.

Since the microtubule density in the internal cytoplasm was extremely high, it was impossible to count them directly. As an alternative approach, their fluorescence intensities lengthwise the radius of HPAEC from the centrosome position to the cell edge were evaluated (Fig. 2G–J). Changes of microtubules fluorescence intensity in cytoplasm of intact cells is described by exponent $f(x) = ae^{-bx}$ ($a = 287.7$ and $b = 0.15$). Exponential decrease is characteristic for perfect radial system with most microtubules diverge from a common center to the cell periphery, centrosome-associated microtubules are

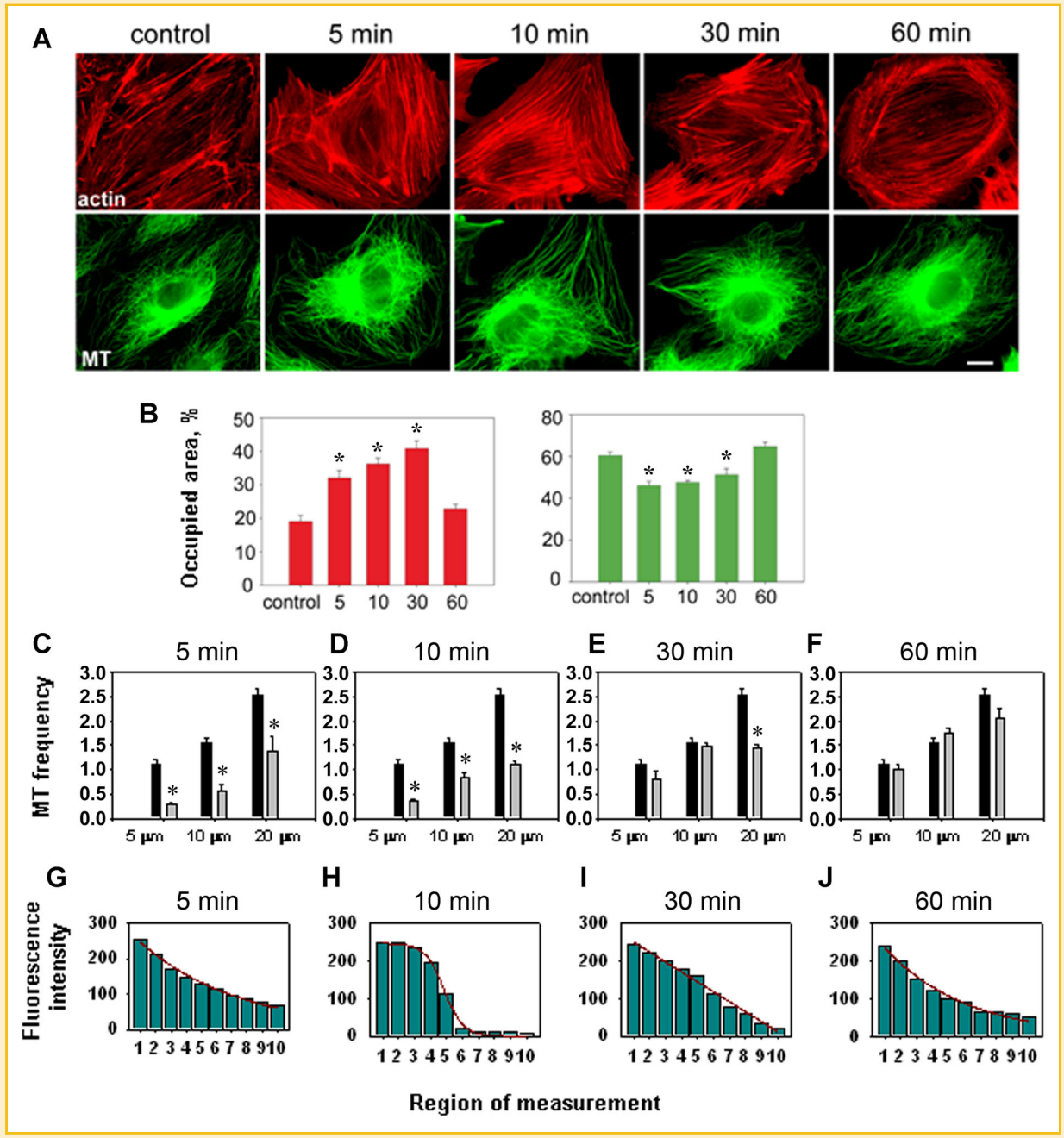

Fig. 2. Effect of thrombin treatment on the cytoskeleton of HPAEC. A: The EC were treated with thrombin (25 nM) for 5, 10, 30, and 60 min, and then stained with Texas Red-conjugated phalloidin for F-actin (top panel) and β-tubulin antibodies for microtubules detection (bottom panel); control cells (0 min) were not treated with thrombin. Scale bar—20 μm. B: Histograms of the stress fibers (left) and microtubules (right) relative area after 5, 10, 30, and 60 min of thrombin (25 nM) treatment. Quantitative analysis of cytoskeleton alterations was performed using MetaMorph software as described in Materials and Methods Section. Data are expressed as a ratio of the cell area covered by stress fibers or assembled microtubules to the whole cell area (the results of three independent experiments). Values significantly different from the control ($P < 0.05$) are indicated by asterisks (n = 3). C–F: The frequency of individual microtubules in lamella of HPAEC treated with thrombin (25 nM): C—5 min; D—10 min; E—30 min; F—60 min of the treatment. All microtubules crossing a random line distant from the edge inside the cell for 5, 10, and 20 μm were counted. The value equal to the number of microtubules crossing the random line per 1 μm of its length was estimated as the criterion for the analysis. Control—black columns; thrombin treatment—grey columns. Values significantly different from the control ($P < 0.001$) are indicated by asterisks (n = 3). G–J: Fluorescence intensity of microtubules along the cell radius from the cell center to its periphery in normal HPAEC (control) and after thrombin treatment. Cells grown on coverslips were treated with 25 nM thrombin for 5, 10, or 60 min. Treated cells were fixed and stained with antibodies to β-tubulin. Fluorescence intensity of microtubules was measured with MetaMorph software in 10 squire areas from centorsome (region 1) to the cell edge (region 10). The curves presented are approximated dependences. G: In control cells, the microtubule fluorescence intensity is the highest in the centrosome area and decreases exponentially from the cell center to its periphery, exponent equation is: f(x) = 287.7E−0.15x. H–J: The distribution of microtubules fluorescence intensity is changed after thrombin treatment, indicating the rearrangement of microtubule system: H—after 5 min of the treatment (nonlinear function described by equation f(x) = 246.4/(1 + E−(x − 4.8)/(−0.6))); I—after 10 min of the treatment (linear regression f(x) = −26.5x + 276.5); J— 60 min of thrombin treatment: recovery to control distribution (exponential decrease of fluorescence intensity (f(x) = 287.4E−0.19x) was very close to that of control EC).

dominate and free microtubules are in less number [Smurova et al., 2007]. However, thrombin treatment changes the dependence which describe fluorescence intensity decrease and, therefore, microtubule redistribution in the internal cytoplasm. After 5 min of the treatment, the reduction of fluorescence intensity from centrosome to the cell edge was approximated by nonlinear function described by the equation $f(x) = a/(1 + e^{-(x-x_0)/b})$, where $x_0 = 4.8$, and coefficient values are: $a = 246.4$ and $b = -0.6$. The diagram demonstrates that the number of microtubules drastically falls in the areas adjacent to centrosome (measurement regions 2, 3, and 4) (Fig. 2H). The number of microtubules located directly around centrosome is not changed. After 10 min of thrombin treatment, the microtubule fluorescence intensity reduction was described by the equation of linear regression $f(x) = ax + b$ with coefficients $a = -26.5$ and $b = 276.5$ (Fig. 2I). According to our published data, this indicated that significant number of free microtubules appeared in the system [Smurova et al., 2007]. After 60 min of incubation of the EC with thrombin, radial microtubules associated with centrosome were dominated; the number of free microtubules was lower. The fluorescence intensity reduction in the EC after 60 min of thrombin treatment was described by exponent $f(x) = ae^{-bx}$ ($a = 287.4$ and $b = 0.19$). Since the values of the equation coefficients obtained in the control EC ($a = 287.7$ and $b = 0.15$) and those obtained at the end of thrombin treatment were very close, microtubule distribution in inner cytoplasm was the same as it was initially, before thrombin treatment (Fig. 2J).

So, not only peripheral microtubules have been rapidly transformed after thrombin treatment. Simultaneously, the number of microtubules in the internal cytoplasm was increased. Distal plus-ends of microtubules considerably enlarge in the internal cytoplasm (after 30 min, microtubules fluorescence intensity in the regions 6 and 7 was significantly higher than that after 10 min of the treatment, and reached the control value) (Fig. 2D). However, at the cell periphery (the regions 8, 9, and 10), the fluorescence intensity after 30 min of the treatment was lower than that in control EC. With further polymerization of distal plus-ends, the number of microtubules increased on the cell periphery and, finally, the microtubule network was completely restored.

The fact that thrombin-activated response of actin cytoskeleton was developed later, than peripheral microtubule depolymerization, indicates that the decrease in microtubules quantity near the cell edge was caused strictly by microtubule depolymerization. A possibility of physical limitation of microtubules growth by some internal obstacles in this area (for example, thick and dense regional bundles of actin filaments) can be ruled out.

PERIPHERAL MICROTUBULES DISASSEMBLY IN THROMBIN-INDUCED EC SIGNALING

In our previous study, we examined a possible link between thrombin-induced EC cytoskeletal remodeling and heterotrimeric G-protein activation [Birukova et al., 2004a]. Our data implicated the involvement of G12 and G13 in thrombin-induced cytoskeletal rearrangement. Overexpression of activated Gα12 and Gα13 led to microtubule depolymerization in the EC, and the area occupied by microtubules decreased to 25% of control [Birukova et al., 2004a]. A counting of individual microtubules in Gα12- and Gα13-transfected EC demonstrated the absence of microtubule distal ends at the distance of 5, 10, and 20 μm from the cell edge (Fig. 3), indicating that the most dramatic destruction of microtubules occurred at the cell periphery.

Thrombin treatment leads to the activation of RhoA and its effector, Rho-kinase (ROCK), stimulating stress fiber formation [Birukova et al., 2004b]. ROCK inhibitor, Y-27632, did not affect morphology of control EC (Fig. 4A), but decreased the quantity of actin filaments (Fig. 4A,B). Y-27632 had a protective effect on microtubule system in thrombin-stimulated HPAEC, suggesting changes in dynamic properties of microtubules. At maximal permeability increase (25 nM thrombin, 30 min, Fig. 1A), Y-27632 did not prevent thrombin-induced dynamic microtubules depolymerization, but prevented thrombin-induced stress fiber formation

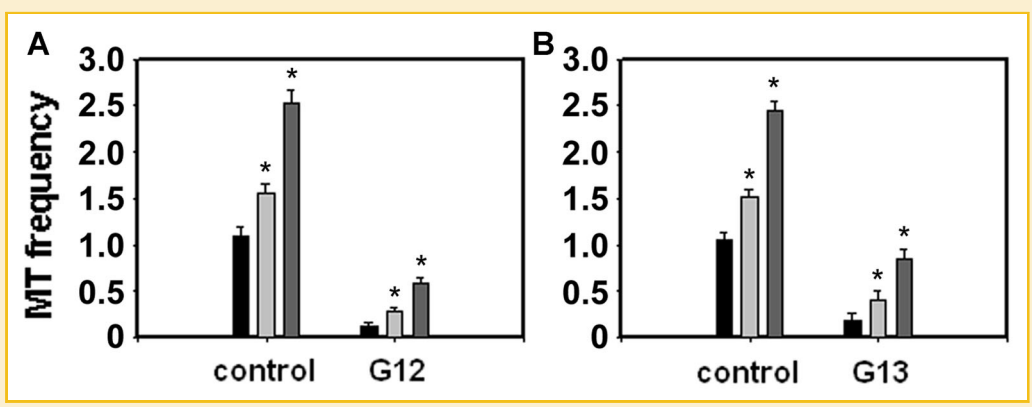

Fig. 3. Effect of G12 and G13 α-subunits overexpression on peripheral microtubules frequency in HPAEC. The cells were transfected with activated HA-tagged Gα12 mutant or with activated HA-tagged Gα13 mutant. Then the cells were double stained with HA-tag antibodies to detect the transfected cells and with β-tubulin antibodies for microtubules detection. The frequency of individual microtubules in lamella distant from the cell edge for 5 μm (black columns), 10 μm (light columns), and 20 μm (dark grey columns) in (A) Gα12-transfected and (B) Gα13-transfected HPAEC. Quantitative analysis of microtubule was performed as described in Materials and Methods Section. Values significantly different from the control ($P < 0.001$) are indicated by asterisks ($n = 3$).

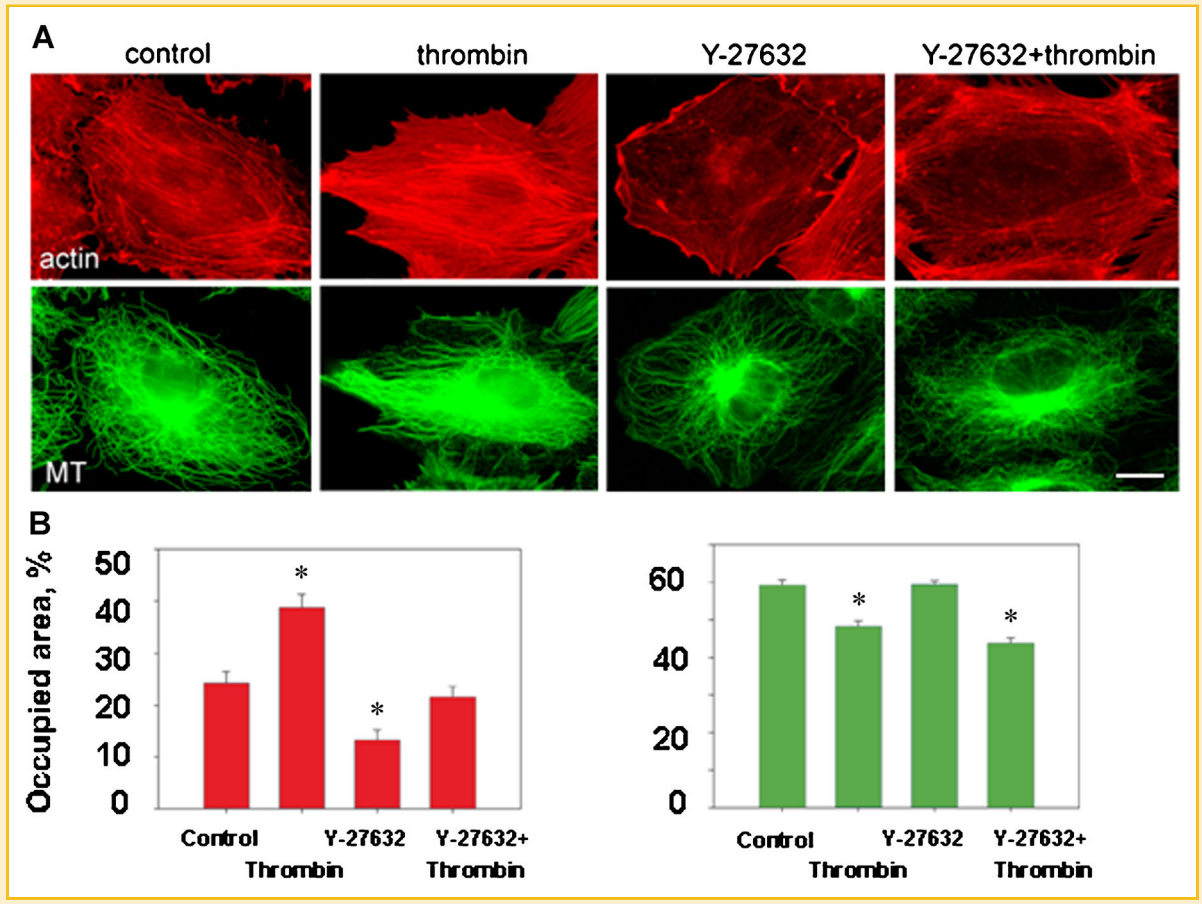

Fig. 4. Effect of Rho-kinase inhibition on microtubules remodeling in thrombin-stimulated HPAEC. A: The cell monolayers were preincubated with vehicle (0.1% DMSO) or Rho-kinase-specific inhibitor Y27632 (5 μM, 1 h) followed by thrombin stimulation (25 nM, 30 min). Actin filaments were stained with Texas Red-conjugated phalloidin. Microtubules were visualized by immunofluorescent staining with β-tubulin antibodies. Scale bar—20 μm. B. Histograms of the stress fibers (left) and microtubules (right) relative area are shown. Morphometric analysis of actin and microtubule system in thrombin-stimulated HPAEC with and without Y27632 pretreatment was assessed using MetaMorph software as described in Materials and Methods Section. Values significantly different from the control ($P < 0.05$) are indicated by asterisks ($n = 3$).

(Fig. 4A,B). Thus, microtubule disruption occurs downstream of heterotrimeric G-proteins activation, but independently of ROCK.

OCCURRENCE OF ENDOTHELIAL BARRIER DYSFUNCTION CORRELATES WITH THE DEGREE OF PERIPHERAL MICROTUBULES DEPOLYMERIZATION

Our data suggest that the disruption of peripheral microtubules may be a common early step in the mechanisms of the endothelial dysfunction. We tested this hypothesis in our next set of experiments using nocodazole, a specific disruptor of microtubules. Previously, we demonstrated that the permeability of the EC monolayer increased in nocodazole-treated cells dose-dependently [Birukova et al., 2004b].

In those experiments, we used nocodazole at the minimal concentration 50 nM which decreased the TER insignificantly (90% of the control level) [Birukova et al., 2004b]. In the present study, the permeability of the EC monolayer was not changed by 50 nM nocodazole (Fig. 5B). Apparently, this concentration is the boundary; therefore the results of the treatment strongly depend on exact conditions of the experiment (different chemicals lots, different lots, and passages of HPAEC used in the experiments as well as different cell culture media used (complete EGM-2 for present study). Thus, here we used 100 nM nocodazole as a minimally effective concentration.

TER, an index of EC monolayer integrity, decreased after 0.5 h of 100 nM nocodazole treatment, while a more pronounced (50% of the control level) and long-lasting change in the permeability were registered in the presence of 200 nM nocodazole. The effect was partially reversible at the concentrations of nocodazole up to 500 nM (70% increase in the monolayer permeability and 10% recovery during 2 h of the treatment).

At 100 nM, nocodazole induced partial disruption of the microtubule network (microtubule depolymerization) at the cell periphery. However, in the internal cytoplasm their distribution was similar to that in control cells (Fig. 5A,C,D). At the cell periphery (5 μm and 10 μm from the cell margin), the numbers of microtubules were 10- and 3-fold lower, respectively (Fig. 5L; Table I). In the central part of the cell, microtubule depolymerization was less pronounced: the microtubules-occupied area was only 25% lower (Table I). Only dynamic microtubules were destroyed upon the treatment, while the number of stable acetylated microtubules were almost the same as in

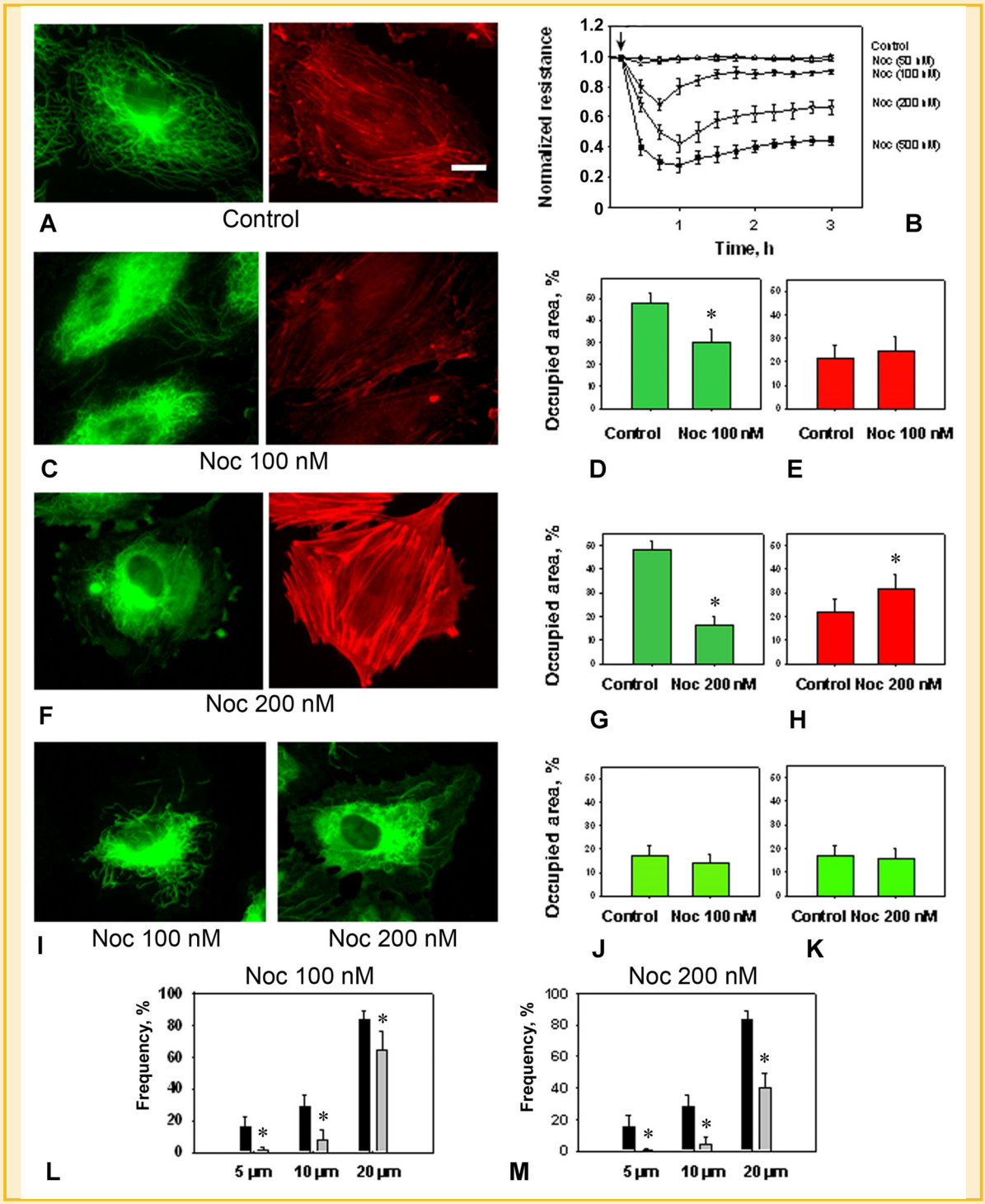

Fig. 5. Effect of nocodazole treatment on the cytoskeleton of HPAEC. A: The cells were treated with either vehicle (0.1% DMSO) or nocodazole 100 nM (C–E) and nocodazole 200 nM (F–H) for 30 min and immunostained with β-tubulin antibodies to detect microtubules (C, F, left panel) and Texas Red-conjugated phalloidin for F-actin detection (C, F, right panel). Scale bar—20 μm. B. HPAEC were plated on gold microelectrodes and were cultured to confluence. At the time indicated by the arrow, the EC were treated with either vehicle (0.1% DMSO) or nocodazole (50, 100, 200, and 500 nM). TER was monitored for 3 h. (D,E,G,H) Histograms of microtubules (D,G), and stress fibers (E,H) relative area during nocodazole treatment. Values significantly different from the control ($P < 0.05$) are indicated by asterisks ($n = 5$). I–K: Acetylated microtubules after nocodozole treatment. I: HPAEC were treated with nocodazole (left—100 nM; right—200 nM) for 30 min and immunostained with acetylated-tubulin antibodies. J,K: Histograms of acetylated microtubules relative area after nocodozole treatment (J—100 nM; K—200 nM). Quantitative analysis of cytoskeleton alterations were performed using MetaMorph software as described in Materials and Methods Section. Data are expressed as a ratio of the cell area covered by stress fibers or assembled microtubules to the whole cell area. All graphs represent the results of three independent experiments. L,M: The frequency of individual microtubules in lamella distant from the cell edge for 5, 10, and 20 μm in control cells (black columns) and cells treated with nocodazole (dark grey columns) (L—100 nM; M—200 nM). Values significantly different from the control ($P < 0.001$) are indicated by asterisks ($n = 5$).

TABLE I. Quantitative Analysis of Microtubules-Occupied Areas in Different Regions of Human EC

	Area occupied by microtubules of interest (%)			
	Total cell area	Central area	Cell periphery	
			10 μm from the margin	5 μm from the margin
Control	47.9 ± 4.1	83.3 ± 5.8	28.3 ± 7.4	15.7 ± 6.6
100 nM nocodazole	30.3 ± 5.5	64.7 ± 11.8	8.1 ± 5.6	1.5 ± 1.3
200 nM nocodazole	16.5 ± 3.8	39.8 ± 9.7	4.4 ± 4.1	Data not shown

control cells (Fig. 5I,J). The population of actin filaments was not changed after 30-min exposure to 100 nM nocodazole (Fig. 5C,E): the cells contained thin disordered stress fibers localized predominantly at the cell periphery similar to the control cells. The area occupied by stress fibers did not differ statistically from control values. The area occupied by actin filaments in the central part of the cell was slightly increased, however, only in the sites separated by a distance of 5 and 10 μm from the cell margin. Taken together, our data suggest that the exposure of the EC to 100 nM nocodazole was accompanied by significant disruption of dynamic, but not stable microtubule network, and had no significant effect on the distribution of actin filaments.

At 200 nM, nocodazole induced significant changes in the microtubule network of HPAEC monolayers (Fig. 5A,F). Quantitative analysis demonstrated that the area occupied by microtubules was decreased nearly threefold (Fig. 5F,G; Table I). In the central part of the cell, the area occupied by the microtubule network was ~2-fold lower than in control cells, and on the cell periphery, the decrease was even more substantial (Table I). Individual microtubules counting revealed significant decrease of microtubules quantity in the cell edge area (Fig. 5M). Similar to 100 nM nocodazole treatment, only dynamic microtubules were destroyed. The distribution of stable acetylated microtubules in 200 nM nocodazole-treated EC was the same as in control cells (Fig. 5I,K). However, the system of actin filaments also underwent certain changes upon 200 nM nocodazole treatment. The population of stress fibers increased, while their thickness and spatial configuration changed: the boundaries of stress fibers were extended far beyond the area adjacent to the central part of the cell (Fig. 5A,F). Quantitative analysis showed that the area occupied by actin filaments was increased by about 50%, especially in the internal cytoplasm (Fig. 5H). The changes in the content of actin filaments in the areas localized at a distance of 5 and 10 μm from the cell margin were insignificant.

Thus, the results obtained suggest that 100 nM nocodazole caused a minimal and short-term disruption of the microtubule network at the cell periphery without any notable effect on the population of stress fibers. However, that was sufficient to produce detectable transient increase in the endothelial permeability. At 200 nM, nocodazole initiated significant depolymerization of dynamic microtubules and formation of additional stress fibers in the internal cytoplasm; these changes were consistent with stable dysfunction of the monolayers. We may conclude that dynamic microtubules are indeed the first target in the development of the vascular endothelium dysfunction. However, the depth of destructive changes at the cell periphery or, more precisely, the number of microtubule ends near the cell margin is also critical for normal functioning of vascular endothelium. If the number of dynamic microtubule ends interacting with the cell cortex drops down below a certain critical level, a cascade of events resulting in the endothelial barrier dysfunction is initiated.

MICROTUBULE PLUS-ENDS GROWTH RATE DECREASED NEAR THE CELL MARGIN DURING THE BARRIER DYSFUNCTION

We first examined microtubule dynamics in HPAEC by time-lapse imaging of EB3-GFP comets movement [Alieva et al., 2010] using ImageJ software that enable tracking and analysis of all growing microtubules. Using this approach, here we were able to directly quantify the microtubule plus ends growth rate in living human EC after nocodazole treatment. Based on the deviation from the mean rate of microtubules growth, we demonstrated, for the first time, that mean growth rate near the cell margin has extremely changed after nocodazole application.

Histograms of microtubule growth rate distribution were obtained by tracking EB3-GFP comets at microtubule plus-ends in (H) before nocodazole (12.27 ± 0.62 μm/min) and (I) (mean growth rate, 5.76 ± 0.05 μm/min).

To visualize microtubule growing ends without the background contributed by the rest of the microtubules, we used EB3-GFP as a marker of growing distal tips of microtubules [Alieva et al., 2010]. Microtubule growth rates were obtained by tracking EB3-GFP comets at the plus-ends. Using this model, we measured microtubule growth rate near the cell periphery before and after induction of the barrier dysfunction in living HPAEC by 100 nM nocodazole (Fig. 6).

Quantitative analysis revealed that microtubule growth rate near the cell margin in untreated cells was more than twofold higher than that in the EC treated with nocodazole for 4–5 min (Table II). Thus, upon the development of the barrier dysfunction, the microtubule plus ends growth rate was significantly decreased.

DISCUSSION

DISASSEMBLY OF PERIPHERAL MICROTUBULES PRECEDES FURTHER CYTOSKELETAL REORGANIZATION DURING THROMBIN-INDUCED BARRIER DYSFUNCTION

An edemagenic agent, thrombin, generated at sites of vascular injury, can cause the endothelial barrier dysfunction [Birukova et al., 2004a; Garcia et al., 1995; Lum and Malik, 1996; Mehta and Malik, 2006]. Changes, induced by thrombin, affect both cytoskeleton components: the actin filaments and microtubules [Verin et al., 2001; Gorovoy et al., 2005; Mehta and Malik, 2006]. Here, we study thrombin-induced reorganization of microtubular network in details and present a quantification of these effects (Fig. 2). Total amount of microtubules dropped rapidly (within 5 min of the treatment), and this decrease was due to a microtubules disassembly on the cell periphery, whereas in the central part of the cell, the density of microtubules was changed insignificantly (Fig. 2A–C,H). The actin cytoskeleton response become apparent much later: a maximal density of the

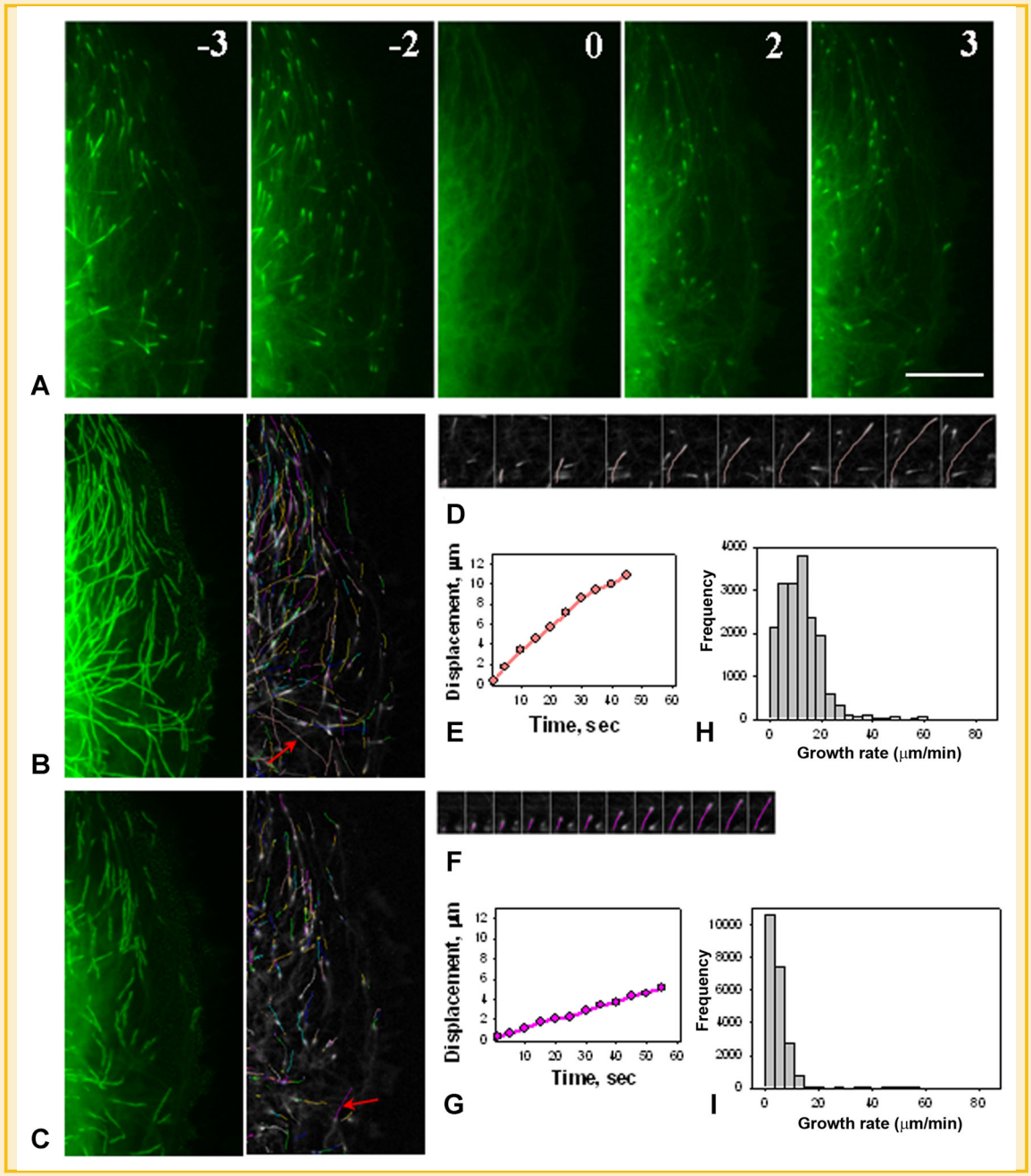

Fig. 6. Microtubule plus-ends growth rate decreased during barrier dysfunction. A–C: EB3-GFP was expressed in the transfected HPAEC and used as a marker of growing microtubule plus ends. EB3-GFP movement was analyzed by time-lapse microscopy. Images were acquired every 1 second. A: EB3-GFP tracks (3 min and 2 min before and after nocodazole application). EB3-GFP is presented at microtubule plus-ends during growth phases but disappears after transition from growth to pause or shortening phase at the moment of nocodazole application (0 min). Time points (min) are shown in right top corner. Scale bar, 10 μm. B, C: EB3 tracks projection obtained by EB3-GFP patches displacement on time-lapse series during 60 sec (left—tracks projection; right—EB3 tracks are colored individually); between 2 and 3 min before (B) and after (C) nocodazole application. D,F: Individual microtubules plus end displacement before (D) and after (F) nocodazole application (5 sec interval between frames). E: Quantification of plus-ends displacement of microtubule (marked by red arrow) shown in D. G: Quantification of plus-ends displacement of microtubule (marked by red arrow) shown in F. H,I: Histograms of microtubule growth rate distribution were obtained by tracking EB3-GFP comets at microtubule plus-ends in HPAEC near the cell margin (H) before nocodazole (mean growth rate, 12.27 ± 0.62 μm/min) and (I) after nocodazole application (mean growth rate, 5.76 ± 0.05 μm/min).

stress fibers was registered after 30 min of thrombin treatment (Fig. 2A,B). Therefore, the decrease in amounts of peripheral microtubules reflected their depolymerization rather than physical prevention of their growth in this area by internal obstacles (thick and dense regional bundles of actin filaments). Moreover, microtubules depolymerization was an essential early event of the barrier disruption: TER reached minimum in 10–15 min of the treatment, before a formation of the stress fibers was completed [Birukova

TABLE II. Microtubule Plus Ends Growth Rates at the HPAEC Periphery

	Growth rate[a]	(μm/min)
Control cells	12.27 ± 0.62	(n = 321)
Nocodazole-treated cells	5.76 ± 0.05[b]	(n = 300)

n = number of microtubules.
[a]Instantaneous rates measured from positions of EB3-GFP dashes in sequential frames of a time-lapse series.
[b]Significant difference from control cells at 99% confidence level. Student's *t*-test was used for statistical analysis.

et al., 2004c]. Furthermore, ROCK inhibition did not prevent thrombin-induced TER decrease even if the stress fibers formation was blocked [Birukova et al., 2004c]. Thus, we can conclude that the microtubules regulate the EC monolayer permeability during initial stages of the thrombin action. The microtubule response is the first phase of barrier dysfunction induced by thrombin, and microtubules are the primary target in the series of rearrangements of the EC fibrillar cytoskeleton. Similarly, microtubules guide the reorganization of the actin cytoskeleton through the differential regulation of focal contact dynamics when the cell shape has been changed during polarization and migration [Small and Kaverina, 2003; Akhmanova et al., 2009].

We have previously shown that thrombin-induced microtubule depolymerization occured after the activation of heterotrimeric G12 and G13 proteins, but preceded ROCK activation which causes further actomyosin contraction and stress fiber formation (Figs. 3–4). Taken together, all these facts strongly suggest the leading role of microtubules in the development of the EC barrier dysfunction. The quantifications presented here as well as in previous reports by us [Birukova et al., 2004b; Smurova et al., 2004] and by others [Gorovoy et al., 2005; Jalimarada et al., 2009; Ren et al., 1998; Shivanna and Srinivas, 2009; Wittmann and Waterman-Storer, 2001] show that microtubules disassembly is not simply implicated in the initial steps of the barrier dysfunction. It also causes a rapid activation of ROCK, that culminates in stress fiber formation. To summarize the experimental data, we propose the following scheme illustrating a cross-talk between microtubules and the actin cytoskeleton in thrombin-induced EC barrier dysfunction (Fig. 7). Interaction of thrombin with transmembrane PAR1 receptor activates G12 and G13 proteins triggering a rapid microtubule depolymerization near the cell margin followed by an activation of RhoA and its effector, ROCK. ROCK, in turn, stimulates myosin light chain phosphorylation, which leads to stress fiber formation and cell contraction, resulting in the endothelial dysfunction.

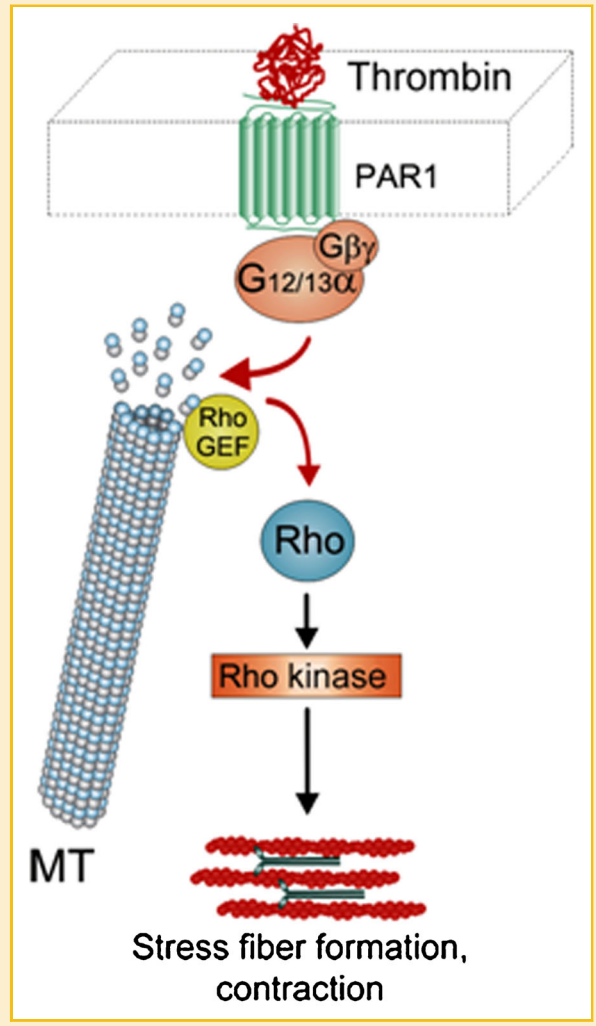

Fig. 7. Proposed scheme of thrombin-induced pathways in fibrillar cytoskeleton regulation. Interaction of thrombin with PAR1 receptor, located on the cell membrane, accompanied with G12 and G13 activation following by rapid microtubule depolymerization near the cell margin results in activation of Rho and its effector Rho-kinase. Rho-kinase regulates myosin light chain phosphorylation, which leads to stress fiber formation and cell contraction, resulting in endothelial dysfunction.

DEPOLYMERIZATION OF MICROTUBULES IS ESSENTIAL AND SUFFICIENT EVENT IN THE DEVELOPMENT OF THE ENDOTHELIAL BARRIER DYSFUNCTION

Specific nocodazole-dependent depolymerization of microtubules itself was sufficient to induce the pathways typical for the barrier dysfunction (Fig. 5). Moreover, the EC dysfunction had a direct correlation with the levels of depolymerization of the peripheral microtubules (Fig. 5A–D,F,G,L,M). The EC TER decrease was registered even at minimal destructions of the peripheral microtubules, while actin filament system still had no changes (Fig. 5B,C).

The observed dramatic decline in the microtubule number in the lamella of the thrombin-treated (Figs. 2–5) or nocodazole-treated EC is possible due to: (i) the limitation of the microtubule plus ends growth in the internal cytoplasm (microtubules growing from the centrosome do not reach the cell edge) or (ii) fast microtubule plus ends disassembly near the cell margin (the absence of pauses and increased frequency of catastrophes). In particular, we observed the second mechanism in live cells time-lapse sequences (Fig. 6), while studied how nocodazole changed the microtubule behavior provoking fast shortening of microtubules ends and their removal from the cell margin region. Nocodazole-induced disassembly of peripheral microtubules resulted in a dramatic decrease of dynamic plus ends number near the cell membrane and, therefore, reduced the frequency of targeting and impaired the relationship between fibrillar components of the cytoskeleton and adhesive cellular structures.

Apparently, according to our data, there is a minimal amount of microtubules exists in the area of cell–cell contacts, providing an interaction with VE-cadherin adherent junctions (AJ) to support the barrier function. The barrier-disruptive cascade can be activated, if the amount of microtubules in the contact area drops below the critical level. Therefore, dynamic plus ends of individual microtubules are involved in the regulation of the cell–cell contacts of the EC, in addition to their regulation of the focal adhesions in fibroblasts [Small and Kaverina, 2003].

Since dynamic microtubules regulate the local concentration of E-cadherin at cell–cell contacts in some types of cells [Stehbens et al., 2006], it is possible to assume that dynamic microtubules can also regulate VE-cadherin AJ in the EC. Thus, a decrease in the number of microtubules in the cell–cell contact area may be critical for VE-cadherin AJ dynamics and sufficient for barrier dysfunction. Interestingly, even changes in microtubules dynamic properties (e.g., peripheral microtubule plus ends velocity decrease) may result in the EC dysfunction. Such changes are characteristic for a number of cell processes in vitro under normal conditions. It is known, for example, that during mitosis, the interphase network of microtubules is reorganizing into a bipolar spindle, and the half-life of microtubules changes from 5–10 to 0.5–1 min [McNally, 1996]. On the other hand, the stability of microtubules increases significantly during cell differentiation [Bulinski and Gundersen, 1991; Zhang et al., 2009]. Dynamic microtubules control cell organization and polarity as well as cell movement and migration [Wen et al., 2004; Bartolini et al., 2008; Schmoranzer et al., 2009], and dynamic microtubule plus ends interactions with cell-substrate and cell–cell adhesions are significant for this regulation [Akhmanova et al., 2009; Broussard et al., 2008; Carramusa et al., 2007; Efimov and Kaverina, 2009; Efimov et al., 2008; Stehbens et al., 2006].

We have previously demonstrated that the development of the endothelial dysfunction induced by thrombin and a number of other agents accompanied by microtubule depolymerization at the cell periphery [Birukova et al., 2004a,b]. Such microtubule depolymerization occurred within first minutes of the treatment, before any changes in actin filament system could be detected [Smurova et al., 2008]. Therefore, we suggested that microtubule depolymerization is an essential condition for a development of the barrier dysfunction. If microtubule depolymerization is indeed a key event of the dysfunction development, it was logical to hypothesize that the endothelial dysfunction would occur not only upon specific barrier disruptor treatment, but also due to a direct influence of specific microtubule inhibitor. That is why we used nocodazole (specific microtubule-disruptor) in our experiments, and data obtained have confirmed our hypothesis. Further, our data presented here suggest that even insignificant elimination of microtubules in the cell edge area upon, for example, 100 nM nocodazole treatment, induced a development of the dysfunction. Thus, to initiate the development of the endothelial barrier dysfunction, would be enough to destroy microtubules at the cell periphery decreasing the number of their plus-ends in cell–cell contacts area. Now this fact become more evident: we recently demonstrated [Lucas et al., 2012] that the barrier function restoration was essentially linked to the restoration of normal numbers of microtubules in the area of cell–cell contacts.

Data obtained in HPAEC [Alieva et al., 2010], human umbilical vein endothelial cells [Sehrawat et al., 2008] and bovine corneal endothelium [Jalimarada et al., 2009; Shivanna and Srinivas, 2009] suggest that microtubule dynamics is involved in VE-cadherin AJ regulation and the EC monolayer barrier function in vitro. Since EC monolayers preserve their in vivo function, our data may suggest that microtubules may regulate endothelial barrier function in vivo by similar mechanisms. If this is true, further research in this direction would help to prevent the endothelial dysfunction, a hallmark of a number of the diseases and therapeutic complications. In particular, anti-microtubule drugs, used in cancer therapy, also affect the barrier function of the endothelium [Schwartz, 2009], and their effect on microtubule dynamics in the EC and in cancer cells may be different [Pasquier et al., 2005]. The strategy of the preventing vascular leak in vivo should be based on the compounds which do not disrupt the EC microtubules dynamics, or on the including of the microtubules protectors.

WHAT IS THE PHYSIOLOGICAL ROLE OF MICROTUBULE DYNAMIC INSTABILITY IN THE ENDOTHELIAL CELL?

The discovery of the microtubule dynamic instability phenomenon [Mitchison and Kirschner, 1984] has raised a question about its biological feasibility. "Search-and-Capture" model [Kirschner and Mitchison, 1986] predicted that during transitions between the growth and shortening of the plus ends, microtubules rapidly explore 3D intracellular space and search for targets to interact with and capture.

We first examined dynamic microtubules behavior in living HPAEC by time-lapse imaging of EB3-GFP comets movement [Alieva et al., 2010]. It is well-known, that endothelial monolayers in vitro are very labile: they easily lose morphology under light or after transfection. Thus, a possibility to get artifacts after transfection is considerable. We were able to find optimal experimental conditions to preserve normal morphology of the EC after transfection and in the process of image recording to study microtubule dynamics in living HPAEC. Originality of our present work is a study of microtubule dynamics under conditions of the barrier dysfunction development in living HPAEC which was done for the first time. We directly quantified the microtubule plus ends growth rate in living nocodazole-treated HPAEC and demonstrated that mean growth rate near the cell margin has extremely decreased (from 12.27 ± 0.62 to 5.76 ± 0.05 μm/min) within the first minutes of nocodazole-induced endothelial barrier dysfunction.

A novelty of our data presented in Figure 6 is a direct demonstration of changes in microtubule dynamics in living EC. We are able to visualize, observe, and quantify them right from the very beginning of the development of the barrier dysfunction. Only such a technically challenging approach allows concluding with a confidence that microtubule network response occurs immediately after the disruptive stimulus, whereas changes in the actin system are induced later. In this context, a nature of the barrier-disrupting stimulus is not very important. The most important fact is that very early stages or the endothelial permeability disturbance link to an impairment of dynamic properties of microtubules in cell–cell contact zone. To the best of our knowledge, these data are unique and have never been published before.

Our results demonstrate that dynamic microtubules play essential role in the behavior of human EC monolayers. According to our previous data, the barrier dysfunction is accompanied with peripheral microtubules disappearance [Birukova et al., 2004a,b; Smurova et al., 2004]. The majority of microtubules in HPAEC are highly dynamic [Alieva et al., 2010], and these dynamic microtubules are capable of adjusting existing contacts and can also adjust endothelial permeability [Alieva et al., 2010]. Present study suggests that the barrier-disruptive treatment leads not only to the disappearance of peripheral microtubules. The entire system of microtubules has been changed: microtubules growing out of centrosome become significantly shorter. Such shortening is possible if microtubules do not reach the cell periphery due to decrease of either plus end growth rate or shortening of the processive growth phase. This may also happen if microtubules rapidly shorten reaching the cell periphery (due to the absence of pauses and increased frequency of catastrophes at the cell periphery). The calculations of the plus end growth rates indicate that at least one of the explanations is correct: upon the development of the barrier dysfunction induced by nanomolar concentrations of nocodazole, the plus end growth rates were dropped markedly. As the result, the plus ends, apparently, cannot reach the cell periphery, and, therefore, dynamic microtubules were not accumulated near the cell margin. Cell–cell contacts in lung epithelial cells were reported to stabilize the dynamic behavior of microtubule plus-ends [Waterman-Storer et al., 2000]. We suppose that in the HPAEC monolayer, where VE-cadherin AJ are well-structured, dynamic microtubules may interact with AJs. This interaction may lead to microtubule stabilization in the area of the cell–cell contact. On the other side, nocodazole-induced microtubule dynamics changes can potentially destabilize VE-cadherin AJs by decreasing their reiterative targeting. We can conclude that the regulation of the endothelial monolayer permeability is one of possible physiological roles for microtubules dynamic instability in interphase cells.

ACKNOWLEDGMENTS

The authors are grateful to Dr. T. Voyno-Yasenetskaya (University of Illinois at Chicago) for providing Gα12 and Gα13 constructs and Dr. A. Akhmanova (Utrecht University, Utrecht, The Netherlands) for providing the EB3-GFP plasmid. We thank Mrs. Zheng Hong Fan for assistance with HPAEC cultivation and Dr. Kyung-Mi Kim for assistance with molecular biology procedures. We also thank Dr. I. Vorobjev (Moscow State University, Moscow, Russia) for the opportunity to work with MetaMorph software (Universal Imaging). This work was supported by Russian Foundation for Basic Research (Grants #09-04-00363 and #12-04-00488) to I.B.A., GHSU CVDI Grant and American Heart Association 11SDG7670035 to E.A.Z., NIH Grants (HL067307, HL080675, and HL101902) to A.D.V., NIH grant R01-GM78373 and American Heart Association Grant-in-Aid #10GRNT4230026 to I.K.

REFERENCES

Akhmanova A, Hoogenraad CC, Drabek K, Stepanova T, Dortland B, Verkerk T, Vermeulen W, Burgering BM, De Zeeuw CI, Grosveld F, Galjart N. 2001. Clasps are CLIP-115 and -170 associating proteins involved in the regional regulation of microtubule dynamics in motile fibroblasts. Cell 104:923–935.

Akhmanova A, Stehbens SJ, Yap. AS. 2009. Touch, grasp, deliver and control: Functional cross-talk between microtubules and cell adhesions. Traffic 10:268–274.

Alieva IB, Zemskov EA, Kireev II, Gorshkov BA, Wiseman DA, Black SM, Verin AD. 2010. Microtubules growth rate alteration in human endothelial cells. J Biomed Biotechnol 2010:671536.

Bartolini F, Moseley JB, Schmoranzer J, Cassimeris L, Goode BL, Gundersen GG. 2008. The formin mDia2 stabilizes microtubules independently of its actin nucleation activity. J Cell Biol 181:523–536.

Bershadsky AD, Ballestrem C, Carramusa L, Zilberman Y, Gilquin B, Khochbin S, Alexandrova AY, Verkhovsky AB, Shemesh T, Kozlov MM. 2006. Assembly and mechanosensory function of focal adhesions: Experiments and models. Eur J Cell Biol 85:165–173.

Birukova AA, Birukov KG, Smurova K, Adyshev D, Kaibuchi K, Alieva I, Garcia JG, Verin AD. 2004a. Novel role of microtubules in thrombin-induced endothelial barrier dysfunction. FASEB J 18:1879–1890.

Birukova AA, Smurova K, Birukov KG, Kaibuchi K, Garcia JG, Verin AD. 2004b. Role of Rho GTPases in thrombin-induced lung vascular endothelial cells barrier dysfunction. Microvasc Res 67:64–77.

Birukova AA, Smurova K, Birukov KG, Usatyuk P, Liu F, Kaibuchi K, Ricks-Cord A, Natarajan V, Alieva I, Garcia JG, Verin AD. 2004c. Microtubule disassembly induces cytoskeletal remodeling and lung vascular barrier dysfunction: Role of Rho-dependent mechanisms. J Cell Physiol 201:55–70.

Bogatcheva NV, Garcia JG, Verin AD. 2002. Molecular mechanisms of thrombin-induced endothelial cell permeability. Biochemistry (Mosc) 67:75–84.

Broussard JA, Webb DJ, Kaverina I. 2008. Asymmetric focal adhesion disassembly in motile cells. Curr Opin Cell Biol 20:85–90.

Bulinski JC, Gundersen GG. 1991. Stabilization of post-translational modification of microtubules during cellular morphogenesis. Bioessays 13:285–293.

Carramusa L, Ballestrem C, Zilberman Y, Bershadsky AD. 2007. Mammalian diaphanous-related formin Dia1 controls the organization of E-cadherin-mediated cell–cell junctions. J Cell Sci 120:3870–3882.

Cattan CE, Oberg KC. 1999. Vinorelbine tartrate-induced pulmonary edema confirmed on rechallenge. Pharmacotherapy 19:992–994.

Cook TA, Nagasaki T, Gundersen GG. 1998. Rho guanosine triphosphatase mediates the selective stabilization of microtubules induced by lysophosphatidic acid. J Cell Biol 141:175–185.

Daub H, Gevaert K, Vandekerckhove J, Sobel A, Hall. A. 2001. Rac/Cdc42 and p65PAK regulate the microtubule-destabilizing protein stathmin through phosphorylation at serine 16. J Biol Chem 276(3):1677–1680.

Dudek SM, Garcia JG. 2001. Cytoskeletal regulation of pulmonary vascular permeability. J Appl Physiol 91:1487–1500.

Efimov A, Kaverina I. 2009. Significance of microtubule catastrophes at focal adhesion sites. Cell Adh Migr 3(3):285–287.

Efimov A, Schiefermeier N, Grigoriev I, Ohi R, Brown MC, Turner CE, Small JV, Kaverina I. 2008. Paxillin-dependent stimulation of microtubule catastrophes at focal adhesion sites. J Cell Sci 121:196–204.

Fuchs E, Karakesisoglou I. 2001. Bridging cytoskeletal intersections. Genes Dev 15:1–14.

Fukata M, Watanabe T, Noritake J, Nakagawa M, Yamaga M, Kuroda S, Matsuura Y, Iwamatsu A, Perez F, Kaibuchi K. 2002. Rac1 and Cdc42 capture microtubules through IQGAP1 and CLIP-170. Cell 109(7):873–885.

Garcia JG, Davis HW, Patterson CE. 1995. Regulation of endothelial cell gap formation and barrier dysfunction: Role of myosin light chain phosphorylation. J Cell Physiol 163:510–522.

Gorovoy M, Niu J, Bernard O, Profirovic J, Minshall R, Neamu R, Voyno-Yasenetskaya T. 2005. LIM kinase 1 coordinates microtubule stability and actin polymerization in human endothelial cells. J Biol Chem 280:26533–26542.

Groeneveld AB. 2002. Vascular pharmacology of acute lung injury and acute respiratory distress syndrome. Vascul Pharmacol 39:247–256.

Ishizaki T, Morishima Y, Okamoto M, Furuyashiki T, Kato T, Narumiya S. 2001. Coordination of microtubules and the actin cytoskeleton by the Rho effector mDia1. Nat Cell Biol 3:8–14.

Jaffe AB, Hall. A. 2005. Rho GTPases: Biochemistry and biology. Annu Rev Cell Dev Biol 21:247–269.

Jalimarada SS, Shivanna M, Kini V, Mehta D, Srinivas SP. 2009. Microtubule disassembly breaks down the barrier integrity of corneal endothelium. Exp Eye Res 89:333–343.

Jordan MA, Wilson L. 2004. Microtubules as a target for anticancer drugs. Nat Rev Cancer 4(4):253–265.

Kirschner MW, Mitchison T. 1986. Microtubule dynamics. Nature 324:621.

Komarova YA, Mehta D, Malik AB. 2007. Dual regulation of endothelial junctional permeability. Sci STKE 2007:re8.

Lucas R, Yang G, Gorshkov BA, Zemskov EA, Sridhar S, Umapathy NS, Jezierska-Drutel A, Alieva IB, Leustik M, Hossain H, Fischer B, Catravas JD, Verin AD, Pittet JF, Caldwell RB, Mitchell TJ, Cederbaum SD, Fulton DJ, Matthay MA, Caldwell RW, Romero MJ, Chakraborty T. 2012. Protein kinase C-alpha and arginase I mediate pneumolysin-induced pulmonary endothelial hyperpermeability. Am J Respir Cell Mol Biol 47:445–453.

Lum H, Malik AB. 1996. Mechanisms of increased endothelial permeability. Can J Physiol Pharmacol 74:787–800.

McNally FJ. 1996. Modulation of microtubule dynamics during the cell cycle. Curr Opin Cell Biol 8:23–29.

Mehta D, Malik AB. 2006. Signaling mechanisms regulating endothelial permeability. Physiol Rev 86:279–367.

Mitchison T, Kirschner M. 1984. Dynamic instability of microtubule growth. Nature 312:237–242.

Palazzo AF, Cook TA, Alberts AS, Gundersen GG. 2001. mDia mediates Rho-regulated formation and orientation of stable microtubules. Nat Cell Biol 3:723–729.

Pasquier E, Honore S, Pourroy B, Jordan MA, Lehmann M, Briand C, Braguer D. 2005. Antiangiogenic concentrations of paclitaxel induce an increase in microtubule dynamics in endothelial cells but not in cancer cells. Cancer Res 65:2433–2440.

Ren Y, Li R, Zheng Y, Busch H. 1998. Cloning and characterization of GEF-H1, a microtubule-associated guanine nucleotide exchange factor for Rac and Rho GTPases. J Biol Chem 273:34954–34960.

Rodriguez OC, Schaefer AW, Mandato CA, Forscher P, Bement WM, Waterman-Storer CM. 2003. Conserved microtubule–actin interactions in cell movement and morphogenesis. Nat Cell Biol 5:599–609.

Schmoranzer J, Fawcett JP, Segura M, Tan S, Vallee RB, Pawson T, Gundersen GG. 2009. Par3 and dynein associate to regulate local microtubule dynamics and centrosome orientation during migration. Curr Biol 19:1065–1074.

Schwartz EL. 2009. Antivascular actions of microtubule-binding drugs. Clin Cancer Res 15:2594–2601.

Sehrawat S, Cullere X, Patel S, Italiano J, Jr., Mayadas TN. 2008. Role of Epac1, an exchange factor for Rap GTPases, in endothelial microtubule dynamics and barrier function. Mol Biol Cell 19:1261–1270.

Shivanna M, Srinivas SP. 2009. Microtubule stabilization opposes the (TNF-alpha)-induced loss in the barrier integrity of corneal endothelium. Exp Eye Res 89:950–959.

Small JV, Kaverina I. 2003. Microtubules meet substrate adhesions to arrange cell polarity. Curr Opin Cell Biol 15:40–47.

Smurova KM, Alieva IB, Vorob′ev. IA. 2007. Free and centrosome-attached microtubules: Quantitative analysis and the modeling of two-component system. Tsitologiia 49:270–279.

Smurova KM, Biriukova AA, Garcia JG, Vorob′ev IA, Alieva IB, Verin AD. 2004. Reorganization of microtubule system in pulmonary endothelial cells in response to thrombin treatment. Tsitologiia 46:695–703.

Smurova KM, Biriukova AA, Verin AD, Alieva IB. 2008. The microtubule system in endothelial barrier dysfunction: Disassembly of peripheral microtubules and microtubules reorganization in internal cytoplasm. Tsitologiia 50:49–55.

Stehbens SJ, Paterson AD, Crampton MS, Shewan AM, Ferguson C, Akhmanova A, Parton RG, Yap. AS. 2006. Dynamic microtubules regulate the local concentration of E-cadherin at cell–cell contacts. J Cell Sci 119:1801–1811.

Stepanova T, Slemmer J, Hoogenraad CC, Lansbergen G, Dortland B, De Zeeuw CI, Grosveld F, van Cappellen G, Akhmanova A, Galjart N. 2003. Visualization of microtubule growth in cultured neurons via the use of EB3-GFP (end-binding protein 3-green fluorescent protein). J Neurosci 23:2655–2664.

van Nieuw Amerongen GP, van Delft S, Vermeer MA, Collard JG, van Hinsbergh VW. 2000. Activation of RhoA by thrombin in endothelial hyperpermeability: Role of Rho kinase and protein tyrosine kinases. Circ Res 87:335–340.

Verin AD, Birukova A, Wang P, Liu F, Becker P, Birukov K, Garcia JG. 2001. Microtubule disassembly increases endothelial cell barrier dysfunction: Role of MLC phosphorylation. Am J Physiol Lung Cell Mol Physiol 281:L565–574.

Voyno-Yasenetskaya TA, Pace AM, Bourne HR. 1994. Mutant alpha subunits of G12 and G13 proteins induce neoplastic transformation of Rat-1 fibroblasts. Oncogene 9:2559–2565.

Waterman-Storer CM, Salmon WC, Salmon ED. 2000. Feedback interactions between cell–cell adherens junctions and cytoskeletal dynamics in newt lung epithelial cells. Mol Biol Cell 11:2471–2483.

Wen Y, Eng CH, Schmoranzer J, Cabrera-Poch N, Morris EJ, Chen M, Wallar BJ, Alberts AS, Gundersen GG. 2004. EB1 and APC bind to mDia to stabilize microtubules downstream of Rho and promote cell migration. Nat Cell Biol 6:820–830.

Wittmann T, Waterman-Storer CM. 2001. Cell motility: Can Rho GTPases and microtubules point the way? J Cell Sci 114(Pt21):3795–3803.

Zhang T, Zaal KJ, Sheridan J, Mehta A, Gundersen GG, Ralston E. 2009. Microtubule plus-end binding protein EB1 is necessary for muscle cell differentiation, elongation and fusion. J Cell Sci 122(Pt9):1401–1409.

SUPPORTING INFORMATION

Additional supporting information may be found in the online version of this article at publisher's web-site.

Supplementary Fig. S1. The population of stress fibers in the original cell images. Left micrograph, actin filaments stained with a phalloidin-Texas Red conjugate; the area corresponding to polymerized actin is marked with red color (right micrograph). The ratio of the areas with polymerized actin to the whole cell area was determined. The regions in which fluorescence intensity was two or more times higher than the mean background level were selected and taken into account.

Supplementary Fig. S2. The number of actin filaments in three different cell compartments was estimated: (1) the area circumjacent to the cell periphery (5 μm from the cell margin); (2) the area circumjacent to the cell periphery (10 μm from the cell margin), and (3) the inner cell compartment separated by a distance of 10 μm from the cell margin. The ratio of the area occupied by actin filaments to the total area was calculated separately for each area.

The number of stress fibers on the original images was determined by marking the area occupied by polymerized actin (marked with gray color on the left micrograph and red color on the right micrograph) with allowance for all the areas where the fluorescence intensity exceeded the average background level two or more times and with subsequent calculation of the ratio of this selected area to the total cell area. The number of actin filaments in different cell compartments was determined in three different areas (left micrograph).

(1) The area circumjacent to the cell periphery (5 μm from the cell margin);

(2) the area circumjacent to the cell periphery (10 μm from the cell margin);

(3) the inner compartment, i.e., cytoplasm (10 μm from the cell margin) not including the first two areas.

The ratio of the area occupied by actin filaments to the measured area was determined separately for each measured area. The relative area occupied by the microtubule network in different cell compartments was calculated in a similar way.

The relative area occupied by the microtubule network was calculated in a similar way.